Electronic Journal of Structural Engineering

Original Article

Cite this: DOI:10.56748/ejse.26795

Received Date: 26 March 2025
Accepted Date: 20 January 2026

1443-9255
https://ejsei.com/ejse

Punching strength in Slab-Column Connections includes Shear Reinforcement using optimized tree schemes

Wenjuan Liu [a*]

[a] Puyang Institute of Technology, Henan University, Puyang, Henan 457000, China
*Corresponding author: 16639392051@163.com

Abstract

The current work introduces a data-driven model to detect punching strength (Vn) in slab-column junctions with shear reinforcement. For the prediction aim, the data collection was created including nine input parameters based on the punching shear mechanism from literature. This data collection comprises 327 rows of samples. The learning collection (70%), validating collection (15%), and evaluation collection (15%) of the dataset were utilized in particular in the building, validating, and testing stages of the suggested framework. This exploration considered a decision tree (DT) algorithm linked with two hybrid optimized methods, named Manta ray foraging optimization (MRFO) and Victoria Amazonica optimization (VAO), as an optimizer. After further inspection, the VAO-DT scheme recommended in this exploration generated superior outcomes to those of earlier studies included in the current study. Based on the presented literature, the greater R2 and lower RMSE and MAE values indicate that the VAO-DT model produces more robust and dependable outcomes than extreme gradient boosting (XGB) and hybrid form of it. MRFO-DT demonstrated good procedural reliability with R2 quantities of 0.9826, 0.9893, and 0.9858 during training, validation, and appraisal. VAO-DT surpassed MRFO-DT in R2 quantities, with 0.9943, 0.9988, and 0.9954. Although MRFO-DT could receive an acceptable function, the DT model linked with VAO can be recognized as the most potent model for forecasting purposes and can be utilized in practical applications.

Keywords

Slab-column connection, Reinforcement, Punching shear resistance, Decision tree, Optimization

1. Introduction

Critical foundations are at risk of destruction due to insufficient retention, severe environmental conditions leading to steel corrosion, and unforeseen breakdowns in slab-column connections. Fiber-reinforced polymer materials (FRPs) are utilized as substitutes for steel to mitigate challenges associated with steel corrosion. This is attributable to their exceptional properties, including inertness, an excellent strength-to-weight ratio, and commendable efficiency under fatigue situations (Raman et al. 2020; Ali et al. 2021; Xian et al. 2021; Hassankhani and Esmaeili-Falak 2024). In the 1990s, it was crucial to emphasize that FRPs were employed to enhance constructions and continue to have importance in this field (A. et al. 2018; Ye et al. 2022). The existing design principles for slab-column connections, grounded in semi-empirical or empirical methodologies, exhibit deficiencies in terms of physical intuition (Deifalla 2022; Vaziri and Salehipour 2025).

Recent applications of artificial intelligence (AI) and machine learning (ML) have been substantial across multiple regions of civil engineering, including structural evaluation, design optimization, infrastructure monitoring, and maintenance (Esmaeili-Falak et al. 2019; Liang and B. Bayrami 2023; Li et al. 2023; Zhang et al. 2024; Oghli and Esmaeili-Falak 2025). The proposed methodology enables engineers to improve infrastructure safety and quality, optimize project performance, and facilitate more informed decision-making (Sarkhani Benemaran 2023; Afkhami Hoor and Esmaeili-Falak 2024). The integration of AI and ML methodologies has improved access to more dependable resources in construction management, effectively controlled overall costs, and these benefits will ultimately facilitate enhanced project advancement (Zhu, Y.; Huang, L.; Zhang, Z.; Bayrami 2022; Dawei et al. 2023; Katariya et al. 2025). With technological growth, it is anticipated that the dependable performance of AI and ML in conjunction would yield substantial progress and enhance all aspects of civil engineering, including design, construction, and maintenance of structures (Esmaeili-Falak and Benemaran 2024).

Moreover, the ML methodology possesses the capability to sequentially document the binaries with exceptional precision (Gim and Rhee 2021; Lee et al. 2021; Yang et al. 2021). In contrast to the intricate nature of punch shear failure, it is imperative to employ innovative, evidence-based strategies to improve predicting precision (Deifalla 2021a, b). In the past 20-30 years, ML has demonstrated substantial advancements across a range of disciplines (Salem et al. 2018; Salem 2021), including construction engineering (Vu and Hoang 2016; Rafiei and Adeli 2017; Goetzke-Pala et al. 2018; Salehi and Burgueño 2018; Kumarawadu et al. 2024). Conversely, the implementation of ML could be advanced utilizing the experimental dataset pertaining to urban phenomena (Rivandi 2024; Alikhani and Ghiyasi 2025; Karimi and Damirchi 2025; Manshour 2025; Manshour and Lehmann 2025).

In a previous study, scholars addressed the issue of slab-column connections using FRP improvements. Jumaa and Yousif, in their study (Jumaa and Yousif 2018), explored 3 ML forecasting methods, namely Curvilinear Regression examination (NLR), Synthetic Neural Network method (ANN), and GEP, to project the punching shear failure of FRPs. The data collection used for training methods consisted of 269 data. The findings revealed that the ANN approach showcased superior predicting precision compared to the other two methods. In reference (Vu and Hoang 2016), two methods were introduced, one utilizing an ANN and the other utilizing an SVM; both methods underwent training using a data collection containing 82 data. In a study conducted by Metwally (Metwally 2013), a Levenberg–Marquardt Synthetic Neural Network (LM-ANN) were donated to project the punching shear strength of cement-based composite slabs strengthened with different kinds of FRPs. The methodology was developed using a limited dataset including 59 entries. The results of his approach demonstrated superior performance relative to the empirical findings.

1.1 Objective and Contribution

This work developed a mixed optimal scheme for projecting punched shear strength (V_n) of Connections between slabs and columns that incorporate shear reinforcement, according to the literature review mentioned above. To estimate the V_n, many machine learning techniques inspired by tree-based methods were created in this work. First, three training, validating, and testing steps are applied to 327 sets of tests for punching shear conducted on the connections between slabs and columns. that were collected from the literature. Decision Tree (DT) is the tree-based scheme that is considered in this exploration. The literature claims that the DT's precision and efficacy are highly dependent on its hyperparameters, which can be optimally recognized by employing meta-heuristic optimization methods. Two recently expensed approaches, Victoria Amazonica optimization (VAO) and Manta Ray Foraging Optimization ($MRFO$), are chosen for this goal. Decision Tree frameworks were donated as a reliable alternative to numerical formulas for estimating structural acting. The project aims to offer structural engineers a more dependable tool for manufacturing enhanced concrete structures that are safer and more effective by using DT methods that have been tuned using meta-heuristic tactics. This improved capability for forecasting may result in more informed choices about structural

evaluation and design, which lowers the possibility of errors and maximizes the use of resources in building projects.

This article is organized as follows: the data collection description is presented in Part 2. Part 3 presents method development. Part 4 determines *DT* schemes' function metrics. Outcomes and discussion of this exploration are presented in Part 5. A summary is given in Part 6 of this document.

2. Dataset Description

To guarantee superior predictive performance, data-driven methodologies must depend on high-quality, accurate data, especially empirical observations. A thorough examination of the current literature was conducted to investigate the punching strength and failure mechanisms in slab-column connections with various shear enhancement configurations. This examination was founded on a data collection comprising 327 empirical data entries sourced from literature review (Kinnunen 2001; Ferreira et al. 2014; Bartolac et al. 2015; Dam et al. 2017; Jin et al. 2017; Eom et al. 2018; Cantone et al. 2019; Jang and Kang 2019; Lewiński and Więch 2020; Lima et al. 2021; Hugo Dalosto de Oliveira et al. 2022), comparative schemes were created to gain a deeper understanding of the underlying tactics and standards influencing the punching strength of enhanced concrete slabs. The outcomes of some studies (Tran and Kim 2021; Faridmehr et al. 2022; Shen et al. 2022; Mellios et al. 2023; Tamimi et al. 2023; Wu and Zhou 2023) suggested that datasets of comparable sizes could also be viable, potentially yielding precise estimations. The researchers recognized the necessity of meticulously selecting and curating the data to guarantee its quality and representativeness (Hosseinnia et al. 2025). This study encompasses specimens from experiments conducted on bidirectional reinforced concrete beams with shear enhancement. The chosen dataset for estimation is highly suitable for executing this technique. Utilizing empirical data with high estimation precision is highly useful in developing anticipated models that can effectively depict the complex behavior of reinforced concrete structures under punching loads. The academics employed insights from the literature review and empirical data to build comparison frameworks that elucidate the principal standards influencing punching strength, thereby progressing the domain of civil engineering.

Before applying the models, several preprocessing operations were carried out to ensure the reliability and robustness of the dataset. First, randomization was applied to eliminate any potential ordering bias and to guarantee an unbiased distribution of the samples. Next, the statistical distribution of the data was evaluated through two normality checks: the Kolmogorov–Lilliefors (KL) test, which yielded a value of 0.015 (between train and validation), 0.011 (between train and test), and 0.0024 (between validation and test), and the Kolmogorov–Smirnov (KS) test, which returned a value of 0.9131 (between train and validation), 0.904 (between train and test), and 0.9336 (between validation and test). These tests provided insights into the conformity of the dataset with a normal distribution. Finally, Min-Max normalization was conducted to scale the features within a uniform range, thereby enhancing the stability of the training process and improving the performance of the developed predictive models. Three hundred twenty-seven reliable laboratory datasets were meticulously chosen, according to the highest standards necessary for accurate prediction. To get superior outcomes in this investigation, partitioning techniques were employed for data collecting. Of the whole data, 70% pertains to the educational segment (specifically, 231 data points out of 100), while 30% remains unaccounted for. The remaining 96 samples were allocated for validation and testing, with each comprising 15% of the total, amounting to 48 samples apiece. The specified division would have resulted in the attainment of the acquired outcome and an improved data prediction. The evaluation metrics presented in Table 1, including minimum, maximum, standard deviation, kurtosis, range, mean, and media, were then thoroughly assessed using the non-normalized data, providing valuable insights into the statistical properties and characteristics of the dataset. As demonstrated in Table 1, d denotes the adequate depth of the slab, a signifies the radial distance from the column face to the point of support. c represents the equivalent width of the column. ρ_t indicates the proportion of flexural reinforcement present, and $A_{sw,d}$ refers to the cross-sectional area of the shear reinforcement located at the column face depth d. Additionally, f_{lc} is the compressive strength of the concrete, f_y represents the yield strength of flexural reinforcement, and $f_{y,sw}$ is the yield strength of the shear reinforcement. The failure mode of the slabs is indicated by FM (with P_{max} = 0, P_{cs} = 1, and P_{out} = 2) while V_n represents the punching resistance.

To enhance comprehension of the executed procedures, one may employ data visualization techniques, such as the half-pie diagram, which facilitates an engaging visual representation of the data's properties. The provided graphic elucidates the technique and the relationships and patterns among the data and parameters. A key benefit of utilizing this instrument is its accessibility, allowing individuals of varying expertise to comprehend the patterns, connections, and procedural methodologies involved. The diagram depicted is referred to by several names, including half-pipe, polar, and radar charts, and is utilized for visualizing and comparing multivariate data. Each axis in this diagram represents a distinct variable, while the radial grid facilitates the identification of patterns and relationships that may not be immediately evident in alternative visualization methods. This examination uses a polar chart to assess ten parameters, comprising nine input parameters and one outcome parameter. The visual representations provide a clear and concise summary of the data attributes, including the range of the f_y variable, depicted in Fig. 1-g, which is approximately limited to between 270 and 920

Table 1. The features of properties for train, validation, and test levels

Category	Stage	Attribute	Unit	Index						
				Min.	*Max.*	*Range*	*Avg.*	*St. D.*	*Kurt.*	*Skew.*
Input 1	Train	a	m	0.0568	1.435	1.3782	0.861	0.271	0.121	-0.472
	Validation			0.175	1.784	1.609	0.877	0.303	0.835	0.103
	Test			0.175	1.784	1.609	0.852	0.311	0.956	0.064
Input 2	Train	d	m	0.0825	0.474	0.3915	0.162	0.054	5.045	1.608
	Validation			0.1	0.469	0.369	0.166	0.069	7.154	2.285
	Test			0.0825	0.474	0.3915	0.181	0.077	3.580	1.676
Input 3	Train	c	m	0.0354	0.52	0.4846	0.237	0.078	0.430	0.230
	Validation			0.106	0.45	0.344	0.237	0.070	0.459	0.228
	Test			0.0895	0.45	0.3605	0.248	0.081	-0.207	0.081
Input 4	Train	ρ_t	%	0.335	3.02	2.685	1.209	0.477	2.161	1.111
	Validation			0.335	3.02	2.685	1.111	0.427	7.133	1.645
	Test			0.335	2.72	2.385	1.089	0.405	4.073	1.137
Input 5	Train	$A_{sw,d}$	cm^2	1	53.4	52.4	12.859	9.897	3.254	1.696
	Validation			1.56	101.79	100.23	16.928	19.070	10.759	2.956
	Test			1.46	81.43	79.97	15.899	14.521	7.609	2.218
Input 6	Train	f_{lc}	MPa	13.3	92.4	79.1	34.413	13.069	3.790	1.743
	Validation			13.9	66.15	52.25	31.948	10.131	2.215	1.279
	Test			14.6	91.3	76.7	34.015	15.229	5.366	2.066
Input 7	Train	f_y	MPa	270	917	647	521.608	108.353	3.211	1.080
	Validation			270	889	619	525.334	108.296	1.572	0.595
	Test			278	917	639	563.255	121.934	2.035	0.663
Input 8	Train	$f_{y,sw}$	MPa	208	1100	892	481.974	145.129	4.692	1.427
	Validation			280	900	620	481.775	141.162	-0.027	0.627
	Test			278	709	431	473.916	124.029	-1.110	-0.044
Input 9	Train	FM	–	0	2	2	1.048	0.627	-0.451	-0.035
	Validation			0	2	2	1.020	0.654	-0.605	-0.021
	Test			0	2	2	0.917	0.571	0.133	-0.006
Target	Train	V_n	MN	0.147	3.132	2.985	0.907	0.549	1.108	1.181
	Validation			0.259	3.35	3.091	0.927	0.676	3.436	1.722
	Test			0.144	3.08	2.936	1.014	0.617	1.494	1.217

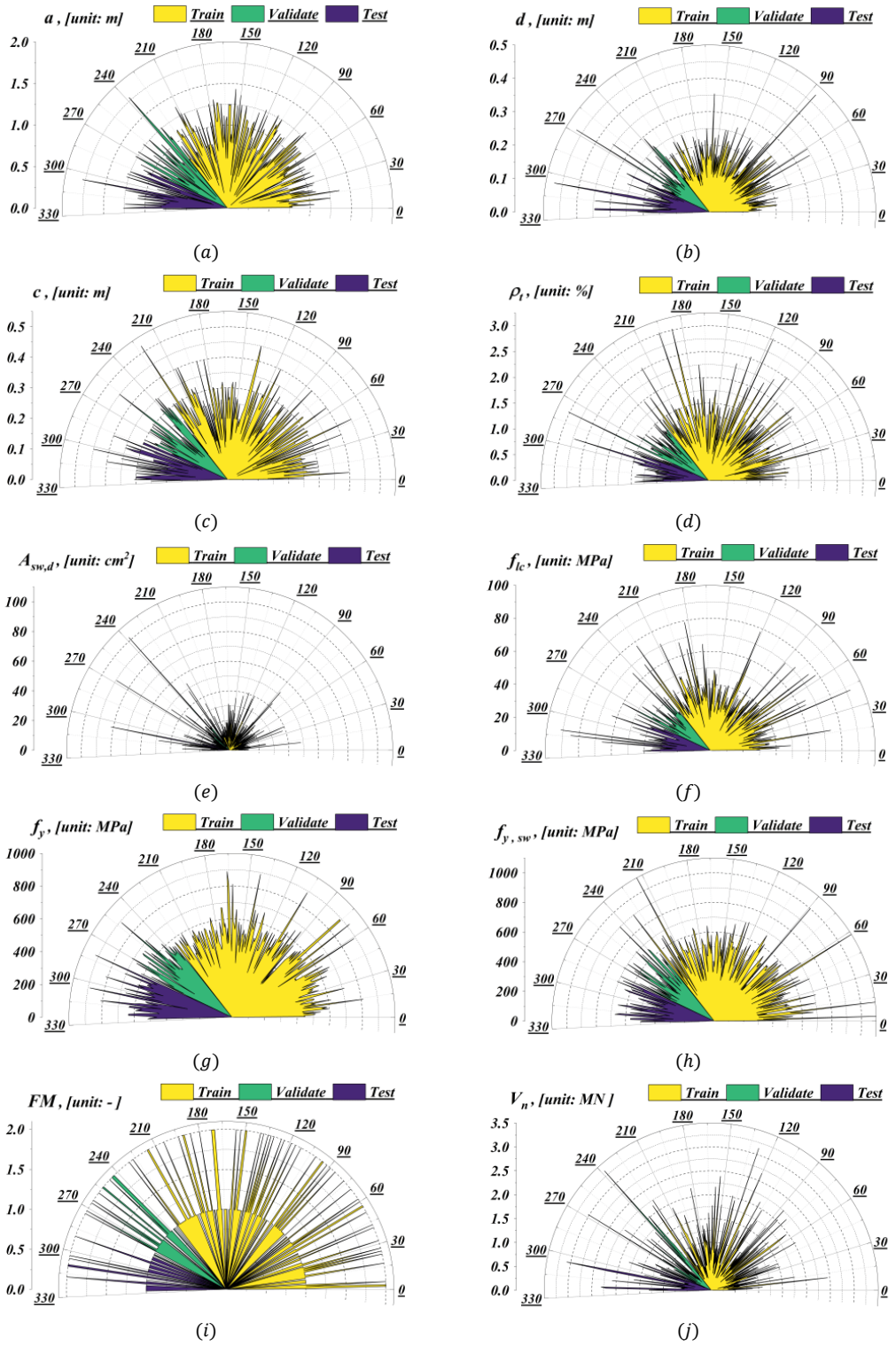

Fig. 1 Distribution plots of parameter, a-i) inputs, g) goal

The researchers have utilized data visualization to examine the Pearson Correlation coefficients among the nine input parameters and the one output parameter, as illustrated in Fig. 2. The Pearson Correlation coefficient is a commonly employed statistical metric that quantifies the linear relationship between two variables, with values spanning from -1 to +1. Elevated positive values indicate a strong positive association, whereas elevated negative values signify a strong inverse link. In contrast, values approaching 0 indicate a weak or insignificant association between the variables. The examination of the correlation matrix indicates the absence of significantly high-value coefficients. Also, four unique pairs, namely $V_n - d$, $V_n - c$, $V_n - A_{sw,d}$, and $A_{sw,d} - d$, exhibit relatively high correlations with quantities of 0.84, 0.52, 0.69, and 0.61, in the same order. The results offer valid insights into the relationships between input and output properties, facilitating the development of more accurate prediction models. The application of data visualization approaches to comprehend correlation coefficients has facilitated readers and scholars in predicting data and parameters, as well as identifying significant connections and their potential implications.

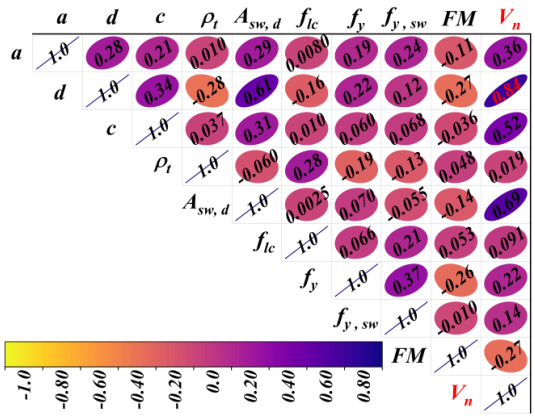

Fig. 2 The Pearson examine (Correlation coefficient)

Furthermore, the Fourier Range Sensitivity Test (FAST) was conducted to improve comprehension of the simulations' sensitivity to the input parameters depicted in Fig. 3. This strategy quantifies the relative importance of each input parameter, resulting in improved outcomes. The results of Fourier Range Sensitivity indicated that the advanced schemes exhibit greater sensitivity to the input parameters. Four parameters demonstrate a Sobol Total (ST) sensitivity index of 0.9, indicating their critical role in influencing the model outputs. Four supplementary parameters have ST numbers between 0.8 and 0.9, signifying a strong, but somewhat reduced, impact on the model's performance. Interestingly, only one parameter, denoted as f_y, exhibits an ST value of 0.66, which is relatively lower than the other inputs. This detailed sensitivity examination provides valuable information for the researchers, allowing them to identify the most crucial input variables that drive the model predictions. By understanding the relative importance of each variable, the scholars may concentrate on precisely defining and integrating the highly sensitive inputs, resulting in more robust and dependable prediction models for civil engineering applications.

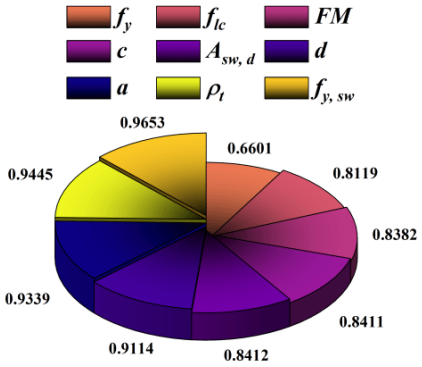

Fig. 3 The feature importance analysis using FAST method

3. Methods

3.1 MRFO

The MRFO enhancement method was initially proposed by Zhao et al. (2020), inspired by the foraging behavior of Manta rays. The manta ray is a well-known marine organism that predominantly feeds on plankton, which comprises minute aquatic organisms. Manta rays employ three separate techniques to discover power supplies: dynasty, whirlwind, and somersault searching.

Dynasty method of searching

Manta rays organize in a linear formation to establish a cohesive strategy for catching plankton during the feeding procedure. The MRFO enhancement strategy asserts that the optimal location is where plankton concentration is highest, acting as the preferred prey for the manta ray lineage to consume. The MRFO approach adjusted the position of each manta ray according to the most exceptional situations and the manta ray preceding it, with the exception of the initial manta ray. Formula (1) delineates the dynasty search refresh mechanism.

$$q_n^{iter+1} = \begin{cases} q_n^{iter} + rand_1\left(q_b^{iter} - q_n^{iter}\right) + \gamma\left(q_b^{iter} - q_n^{iter}\right) n = 1 \\ q_n^{iter} + rand_2\left(q_{n-1}^{iter} - 1_n^{iter}\right) + \gamma\left(q_b^{iter} - q_n^{iter}\right) n = 2, \dots, N \end{cases} \quad (1)$$

$$\gamma = 2 * rand_3 * \sqrt{|log(rand_4)|} \quad (2)$$

The position of the nth manta ray at repetition iter is represented by q_n^{iter}, while $rand_{1,2,3,4}$ are distinct accidentally generated quantities within the range [0, 1]. The weighting agent γ is defined, and q_b^{iter} represents the plankton with the highest density. During the dynasty searching method, the revision of place is influenced by the improved plankton situation and the manta ray that came before in the trail.

Whirlwind method of searching

In the whirlwind method of foraging, manta rays converge to create a helical formation by connecting from the bottom to the top as they recognize areas with the highest concentration of plankton. Each manta ray employs this knowledge to maneuver towards the plankton and track the motion of the manta ray preceding it. Formula (3) quantitatively delineates the whirlwind method revision system.

$$q_n^{iter+1} = \begin{cases} q_b^{iter} + rand_5\left(q_b^{iter} - q_n^{iter}\right) + \alpha\left(q_b^{iter} - q_n^{iter}\right) n = 1 \\ q_b^{iter} + rand_6\left(q_{n-1}^{iter} - q_n^{iter}\right) + \alpha\left(q_b^{iter} - q_n^{iter}\right) n = 2, \dots, N \end{cases} \quad (3)$$

$$\alpha = 2 * e^{rand_8} * \left(\frac{MaxIter - iter + 1}{iter}\right) * sin(2 * \pi * rand_8) \quad (4)$$

The weight factor is represented by ∝, the highest value of repetitions is defined by MaxIter, and $rand_{5,6}$ are the dissimilar manufactured quantities within the range 0 and 1. The MRFO technique depends on this phase as its principal mechanism for discovery and application. Utilizing the apex plankton as a standard, this method can efficiently explore the productive zone adjacent to the current highest resolution, consequently augmenting its usage potential. It provides essential support for enhancing discovery capabilities by requiring manta rays to move to an unintended location within the quest zones, which must be not only remote from their present location but also from the improved prey location. This enables a more comprehensive exploration of the worldwide quest region and assists the MRF method in directing the Manta rays through uncharted territories within the quest zone. This suggested process is illustrated in Eqs. (5) and (6).

$$q_{rp}^{iter} = Lw + rand_9(Up - Lw) \quad (5)$$

$$q_n^{iter+1} = \begin{cases} q_{rp}^{iter} + rand_{10}\left(q_{rp}^{iter} - q_n^{iter}\right) + \alpha\left(q_{rp}^{iter} - q_n^{iter}\right) n = 1 \\ q_{rp}^{iter} + rand_{11}\left(q_{n-1}^{iter} - q_n^{iter}\right) + \alpha\left(q_{rp}^{iter} - q_n^{iter}\right) n = 2, .., N \end{cases} \quad (6)$$

The variable q_{rp}^{iter} denotes an accidentally manufactured situation within the specified boundaries, Up also Lw, which represent the highest and least borders at a specific situation. Meanwhile, $rand_{5,6,7,8,9,10}$, also 11 represent distinct accidental values within the range 0 and1.

Somersault searching method

Somersault method of searching is a common, indigenous, stochastic, and periodic conduct that helps manta rays feed on a larger number of plankton. The situation with the most plankton focused is chosen as the starting dot, and every manta ray orbits around this dot while somersaulting to a different place (Turgut 2020). Formula (7) serves as a numerical depiction of this concept.

$$q_n^{iter+1} = q_n^{iter} + smsf * \left(rand_{12} * q_b^{iter} - (rand_{13} * q_n^{iter})\right) \quad (7)$$

In this exploration, the $SMSF$ is assigned a quantity of 2, denoting the somersault agent, while $rand_{12,13}$ represent two distinct acidentally manufactured values within the range of 0 to 1 (Turgut 2020).

Algorithm 1. MRFO Improvement Method

Keep working until the standards are fulfilled
For $n = 1, \dots, N$ do
If $rand_1 < 0.5$ then
If $\left(\frac{iter}{MaxIter}\right) < rand_5$ then //cyclone foraging
$q_{rp}^{iter} = LW + rand_9(UP - LW)$
$q_n^{iter+1} = \begin{cases} q_{rp}^{iter} + rand_{10}\left(q_{rp}^{iter} - q_n^{iter}\right) + \alpha\left(q_{rp}^{iter} - q_n^{iter}\right) n = 1 \\ q_{rp}^{iter} + rand_{11}\left(q_{n-1}^{iter} - q_n^{iter}\right) + \alpha\left(q_{rp}^{iter} - q_n^{iter}\right) n = 2, .., N \end{cases}$
Else
$q_n^{iter+1} = \begin{cases} q_b^{iter} + rand_5\left(q_b^{iter} - q_n^{iter}\right) + \alpha\left(q_b^{iter} - q_n^{iter}\right) n = 1 \\ q_b^{iter} + rand_6\left(q_{n-1}^{iter} - q_n^{iter}\right) + \alpha\left(q_b^{iter} - q_n^{iter}\right) n = 2, \dots, N \end{cases}$
End if
Else // Chain foraging
$q_n^{iter+1} = \begin{cases} q_n^{iter} + rand_1\left(q_b^{iter} - q_n^{iter}\right) + \gamma\left(q_b^{iter} - q_n^{iter}\right) n = 1 \\ q_n^{iter} + rand_2\left(q_{n-1}^{iter} - 1_n^{iter}\right) + \gamma\left(q_b^{iter} - q_n^{iter}\right) n = 2, \dots, N \end{cases}$
End if
// Compute fitness for n^{th} manta ray $f(q_n^{iter+1})$
If $f(q_n^{iter+1}) < f(q_b^{iter})$ then
$q_b^{iter} = q_n^{iter+1}$
End if
End for
//Somersault foraging
For n = 1, … , N do
$q_n^{iter+1} = q_n^{iter} + smf * \left(rand_{12} * q_b^{iter} - (rand_{13} * q_n^{iter})\right)$
// Compute fitness for n^{th} manta ray $f(q_n^{iter+1})$
If $f(q_n^{iter+1}) < f(q_b^{iter})$ then
$q_b^{iter} = q_n^{iter+1}$
End if
End for
End while

The $MRFO$ algorithm replicates three primary forms of manta ray hunting actions: cyclone hunting, chain hunting, and somersault hunting. Every individual in the community is represented as a manta ray, with its location defined by the vector q_n. Random factors ($rand_i$) are employed to generate variation and avert early convergence. The coefficients α and γ regulate the magnitude of motion towards the optimal known location (q_b) and establish an equilibrium between exploration and extraction. The Somersault Factor (SMF) quantifies the extent of abrupt movement of the manta ray, resulting in an expanded exploration of the solution area. The integration of these three processes endows $MRFO$ with a significant capability for universal quest and the recognition of ideal resolutions to intricate issues.

3.2 Victoria Amazonica Optimization (VAO)

The VAO approach primarily focuses on the dispersion of the predominant crowd, including both foliage and blossoms, as well as their inherent capacity to permeate and expand beyond the external surface (Mousavi 2023). The previously described contest is typically designated as infighting or Γ in its characterization. Moreover, three prevalent impediments hinder the proliferation of plant life. The mortality rate of coleopterans within the flower, inadequate pollination by coleopterans, and a diminish in ambient temperature all contribute to impeding the reproductive success of plants. The aforementioned factors can have negative effects on the procedure in question and are collectively known as φ in this scenario. A higher number of the variable ω signifies a less robust plant. Water lily Aphids, a type of pest, have the possibility to harm plants by feeding on their foliage, resulting in holes. The θ, in this context, represents the danger coefficient being debated. A decrease in the quantity of θ indicates more favorable circumstances for plant growth and development.

Cross-breeding among the beetles living in the lake and a distinct species of water lilies leads to a mutation known as mixture genetic variation, denoted by the η. According to the research by (Mousavi 2023), this transformation may result in an affirmative or adverse outcome, with a 0.2% chance of incidence in every new descendant. The most superior leaf specimen can be distinguished by its significant measurement and robust physical attributes, denoted as α. Furthermore, the VAO method is presented in code sketch below. Method 1 offers the code sketch for VAO.

$$VOA = \sum_{i=1}^{n}\sum_{j=1}^{n}\left(x_{ij}\left[\xi_{ij}, \Gamma_{ij}\right] + \theta + \varphi\right) \times (\eta) \tag{8}$$

In the aforementioned formula, x_{ij} denotes the placement (or decision value) inside the community, whereas the term $\left[\xi_{ij}, \Gamma_{ij}\right]$ signifies arbitrary coefficients or control ranges that illustrate intra-population rivalry and the influence of external situations. These numbers are created arbitrarily to foster variation and prevent the algorithm from becoming ensnared in local minimum. The symbol θ denotes the coefficient of the "disadvantage factor" attributable to environmental factors. ϕ denotes the mutation factor, whereas η signifies the growth rate factor that influences the magnitude of the effect of the aforementioned combination on the final placement.

Algorithm 2. The pseudo-code of VAO during optimization (Mousavi 2023)

Start
Cultivating a crowd of vegetation $xi(i = 1,2,\cdots,n)$.
Calculate the growth ξ_i in x_i.
Calculate the inner contest Γ_i within x_i.
Calculate the disadvantage factor of φ in x_i (accidentally selected from the range of 0.1 to 0.3).
Find the disadvantage agent of Θ for x_i, where x_i is an accidental quantity between 0.1 and 0.3.
Calculate the hybrid death price with a value of $\eta = 0.2$.
If the maximum number of cycles has not been reached.
For $i = 1\ ton\ plants$
For $j = 1\ ton\ plants$
If $\xi_i > \xi_j\ or\ \Gamma_i > \Gamma_j\ for\ x_i (i = 1,2,\ldots,n)$
Plant i is transferred to planet j.
End if
Implement hybrid death rate η.
Utilize the disadvantage factor φ and Θ.
Assess the latest alternatives based on the subordinate price and revise the development accordingly.
End
End
Organize and classify plants to determine the top-performing species worldwide.
Creating the next wave of technology.
End of while
End

The Victoria Amazonica Optimization (VAO) algorithm incorporates a range of biological and environmental characteristics to model the growth and reproductive patterns of the gigantic water lily. Every individual in the population is represented as a plant, with its location in the search space determined by the variables x_{ij}. The coefficients ξ_{ij} and Γ_{ij} denote intrapopulation competition and the influence of environmental factors, accordingly, they are produced randomly to promote diversity and discovery within the quest zone. The agent θ functions as an environmental constraint, while ϕ represents mutation or genetic alteration. Ultimately, the agent η regulates the magnitude of growth and leaf expansion. By integrating these elements, the algorithm effectively balances discovery and utilization, leading to the convergence of ideal answers.

3.3 Base Description of Decision Tree (DT) and Hybrid Schemes

DT is a supervised learning tactic utilized to categorize regression issues and is also frequently employed for ranking issues (Karbassi et al. 2014). The tree contains various classes within its structure. In the absence of a class, the regression method can project the result based on autonomous parameters (Fazeli et al. 2025). A DT is a classifier organized in a tree framework, with internal nodes representing features of a data library (Erdal 2013; Rivandi and Jamili Oskouie 2024). The DT is composed of decision nodes and leaf nodes, with decision nodes having numerous branches to make decisions, and leaf nodes representing the outcomes without any branches. The conclusion laws are indicated by the branches, and each leaf node signifies an outcome. The term "decision tree" is used to describe a framework that resembles a tree, beginning with a root node and branching out into numerous branches, creating a tree-shape creation (Ben Chaabene et al. 2020; Bagherabad et al. 2025). This method involves dividing data specimens at different dots to make decisions. The method in question is designed to identify discrepancies among the anticipated and real quantities at each partitioned segment. These discrepancies are assessed at each partitioned segment, and the parameter exhibiting the least fitness subordinate number is chosen as the splitting dot. This process is then iterated.

Creating a DT model is an attempt to accomplish the goal of creating a flexible and resilient ML technique which can handle regression and classification issues with remarkable endurance and precision. Improving prediction precision and controlling missing data are two of the key goals of deploying DT. Other objectives include enhancing feature significance, scalability, and flexibility. The hyperparameters which substantially impact the efficacy of DT frameworks may be changed using optimization methods or the error and trial approach.

The following are the stages involved in modifying a DT model's hyperparameters:

a. It is possible to modify the following hyperparameters: $\mathrm{Max}_{\mathrm{depth}}$, $Min_{samples\_split}$, $Min_{samples\_leaf}$, $Max_{features}$ and Max_{leaf_nodes}. To ascertain every individual's range, the DT library and released works were examined.
b. A 70/15/15 split was used to divide the dataset into subgroups for learning, validating, and assessing.
c. Subsequently, an optimization technique-based tuning method was taken into consideration. In this work, DT was used in conjunction with two recently created optimization techniques, $MRFO$ and VAO, to modify the hyperparameters.
d. Learning datasets were then introduced to generate initialized schemes. Various mixtures of hyperparameters will be used to train many schemes, and every model's efficacy will be appraised.
e. Following the completion of the search, the outcomes were reviewed to identify the optimal hyperparameters, with attention given to the $RMSE$ values that were specified as the target function.
f. To test the final scheme's efficacy on unknown data, its productivity was assessed on an alternative evaluation set.

4. DT Schemes' Performance Metrics

A number of factors were considered and calculated to evaluate the level of efficacy attained by the developed DT model. All of the following measures made up these measurements: R^2, $RMSE$, normalized root-mean-square ($NRMSE$), Relative absolute error (RAE), MAE, Mean Absolute Scaled Error ($MASE$), Mean Squared Logarithmic Error ($MSLE$), and Mean Relative Error (MRE).

$$R^2 = \left(\frac{\sum_{i=1}^{m}(N_i - \bar{N})(Y_i - \bar{Y})}{\sqrt{[\sum_{i=1}^{m}(N_i - N)^2][\sum_{i=1}^{m}(Y_i - \bar{Y})^2]}}\right) \tag{9}$$

$$RMSE = \sqrt{\frac{1}{m}\sum_{i=1}^{m}(Y_i - N_i)^2} \tag{10}$$

$$NRMSE = RMSE/\bar{D} \tag{11}$$

$$RAE = \frac{\sum_{i=1}^{m}|N_i - Y_i|}{\sum_{i=1}^{m}|N_i - \bar{N}|} \tag{12}$$

$$MAE = \frac{1}{m}\sum_{i=1}^{m}|Y_i - N_i| \tag{13}$$

$$MASE = \frac{\frac{1}{m}\sum_{i=1}^{m}|N_i - Y_i|}{\frac{1}{m-1}\sum_{i=2}^{m}|N_i - N_{i-1}|} \tag{14}$$

$$MSLE = \frac{1}{m}\sum_{i=1}^{m}\left(In(N_i+1)\right) - In(Y_i+1)^2 \quad (15)$$

$$MRE = \frac{1}{m}\sum_{i=1}^{m}\left|\frac{N_i - Y_i}{N_i}\right| \quad (16)$$

The calculations that were done produced the following outcome: The numbers that are displayed are the entire number of observations (m), the predicted value (Y_i), and the meaning of the predicted amount ($\bar{Y}$). The meaning of the actual V_n is represented by $\bar{N}$, while the actual V_n is represented by N_i.

5. Outcomes and Discussion

By combining the DT techniques with the $MRFO$ and VAO procedures, the punching shear resistance (V_n) was determined (abbreviated $VAO-DT$ and $MRFO-DT$, correspondingly). Figure 4 displays the observed and expected V_n values for the $VAO-DT$ and $MRFO-DT$ methods during the validation, learning, and evaluation stages. Additionally, it shows every participant's predicted measured V_n ratio during the course of the exploration. The conclusions drawn from the assessments of the designs acquired during the steps of learning, validating, and assessing the product development technique are shown in Table 2. To increase the accuracy of the integrated schemes, the present research gave each model a score for each measure at each step. The outputs of the present study on produced schemes were also compared with the available research to appraise the reliability and power of the schemes—XGB and $WOA-XGB$ were taken into account (Yan et al. 2024a).

The results indicate that there is considerable potential for both $VAO-DT$ and $MRFO-DT$ to accurately estimate the V_n. In the training, validating, and assessment stages, the $MRFO-DT$ method attained R^2 of 0.9826, 0.9893, and 0.9858, respectively, demonstrating a high level of process dependability. The $VAO-DT$ method outperformed the $MRFO-DT$ technique with regard to R^2 values, as evidenced by the pattern, with 0.9943, 0.9988, and 0.9954 serving as comparable values. Merely relying on this metric to assess model dependability is inadequate. To do this, a comprehensive examination of many measures—including but not limited to $RMSE$, $NRMSE$, RAE, MAE, $MASE$, $MSLE$, and MRE—must be conducted. A smaller value demonstrates a more constant precision in relation to these metrics than a larger one. According to a study of the values produced for these parameters, the $VAO-DT$ approach may provide the lowest values with the maximum degree of reliability. The $VAO-DT$ presented the smallest values of the RAE index during all three stages: training-0.0274, validating-0.0191, and assessment-0.0296. Those numbers proved to be smaller with respect to those values that $MRFO-DT$ reached during the learning, validating, and assessment phases: 0.0589, 0.0554, and 0.0553, respectively. The lowest value generated by the $MASE$ index during the training, validating, and evaluation phases in $VAO-DT$ was 0.04, 0.0292, and 0.0545, respectively. Figures presented established a finer level of precision compared to the values of $MRFO-DT$ achieved through the learning, validating, and assessment stages of 0.0861, 0.0845, and 0.1019, respectively. Based on the ratings provided by the two methods, $VAO-DT$ reveals higher potential than $MRFO-DT$ in every modification stage.

The VOA model is a novel framework particularly engineered to achieve equilibrium between discovery and utilization, including biologically inspired mechanisms such as competition, mutation, and adaptive development. This equilibrium is crucial in the hyperparameter enhancement of decision tree-based models, as improper tuning can severely undermine estimation accuracy. The findings collected further highlighted the superiority of this novel strategy, especially in comparison to existing algorithms. By amalgamating competitive and mutational mechanisms, VAO sustains population variety while perpetually converging towards ideal resolutions. This trait declines the likelihood of stagnation in local ideals and boosts convergence robustness.

The comparative performance of the models based on the coefficient of determination (R^2) highlights the superiority of the $VAO-DT$ approach over SVR, ANN, and RBF across all datasets. In the training phase, $VAO-DT$ achieved an R^2 of 0.9943, which is higher than SVR (0.8461), ANN (0.9472), and RBF (0.8440). Similarly, in the validation phase, $VAO-DT$ maintained excellent accuracy (R^2 = 0.9988), compared to SVR (0.9178), ANN (0.9739), and RBF (0.9183). The testing results further confirm the robustness and generalizability of $VAO-DT$, with an R^2 of 0.9954, while SVR, ANN, and RBF recorded lower values of 0.9157, 0.9730, and 0.8998, respectively. In terms of $RMSE$, $VAO-DT$ consistently produced the lowest error across all stages. For the training phase, $VAO-DT$ achieved an $RMSE$ of 0.0416, outperforming SVR (0.2273), ANN (0.1398), and RBF (0.2328). During validation, $VAO-DT$ reached 0.0240, compared to SVR (0.2021), ANN (0.1229), and RBF (0.2081). Finally, in the testing phase, $VAO-DT$ maintained a superior performance with an $RMSE$ of 0.0428, while SVR, ANN, and RBF showed higher errors of 0.1792, 0.1143, and 0.2019, respectively.

A close comparison with the literature is provided, considering schemes XGB and $WOA-XGB$, to validate the reliability of the schemes (Yan et al. 2024b). From a careful analysis of Table 2, it is noticed that the $VAO-DT$ model recommended in the current study outperformed previous studies included in the corpus of the present research. This result was achieved using similar measures of R^2, MAE, and $RMSE$ derived from the train and evaluation data phases. The outcomes generated by the better model, $VAO-DT$, are more reliable and robust than those from XGB and $WOA-XGB$, as evidenced by the higher R^2 and lower $RMSE$ and MAE values found by (Yan et al. 2024b). For instance, there is an increase in R^2 for $WOA-XGB$ (Yan et al. 2024b) in the course of assessment from 0.9642 to 0.9954 and at learning from 0.994 to 0.9943. Error-based indices, which follow $RMSE$ measures, also decreased in this exploration from 0.125 to 0.0428 at the evaluation stage and from 0.045 to 0.0416 when learning. A closer look can be done between the outcomes of $VAO-DT$ and XGB (Yan et al. 2024b), in learning, validating and assessing data sets with noted improvements boosting the values of R^2 while decreasing the values of $RMSE$.

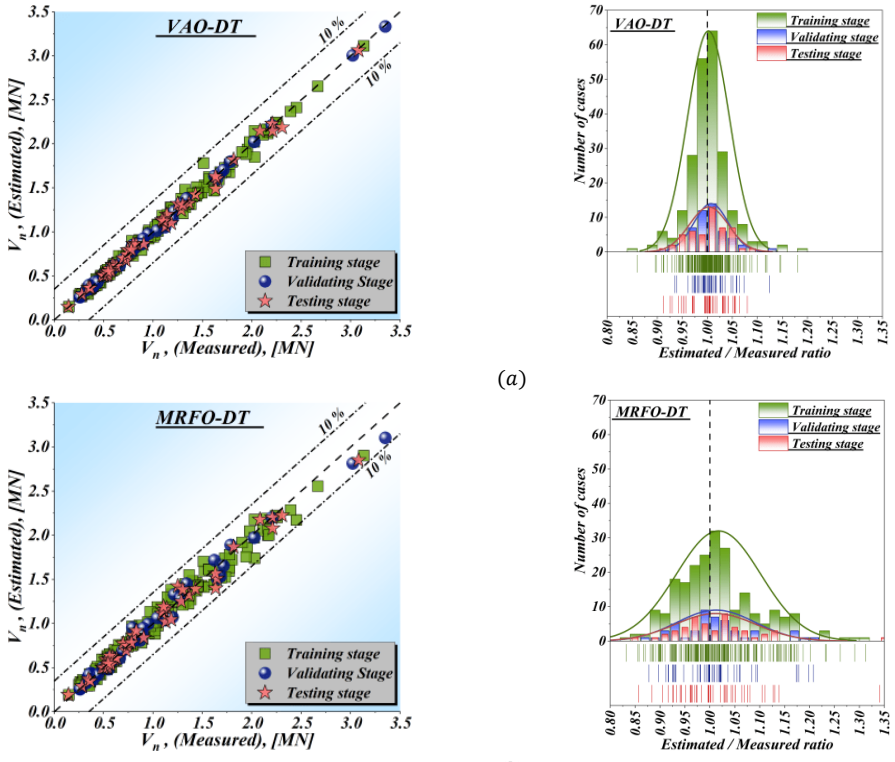

Fig. 4 The integrated schemes' outcomes

Table 2. The integrated schemes' outcomes

Metrics	Stage	Best position	Present study							Literature	
			$VAO-DT$	Score	$MRFO-DT$	Score	SVR	ANN	RBF	XGB (Yan et al. 2024b)	$WOA-XGB$ (Yan et al. 2024b)
R^2	Train	Large	0.9943	2	0.9826	1	0.8461	0.9472	0.8440	0.884	0.994
	Validation		0.9988	2	0.9893	1	0.9178	0.9739	0.9183		
	Test		0.9954	2	0.9858	1	0.9157	0.9730	0.8998	0.8682	0.9642
$RMSE$	Train	Low	0.0416	2	0.0752	1	0.2273	0.1398	0.2328	0.203	0.045
	Validation		0.024	2	0.0773	1	0.2021	0.1229	0.2081		
	Test		0.0428	2	0.078	1	0.1792	0.1143	0.2019	0.242	0.125
$NRMSE$	Train	Low	0.0139	2	0.0252	1					
	Validation		0.0078	2	0.025	1					
	Test		0.0146	2	0.0266	1					
RAE	Train	Low	0.0274	2	0.0589	1					
	Validation		0.0191	2	0.0554	1					
	Test		0.0296	2	0.0553	1					
MAE	Train	Low	0.0248	2	0.0532	1				0.125	0.033
	Validation		0.018	2	0.0519	1					
	Test		0.03	2	0.056	1				0.149	0.087
$MASE$	Train	Low	0.04	2	0.0861	1					
	Validation		0.0292	2	0.0845	1					
	Test		0.0545	2	0.1019	1					
$MSLE$	Train	Low	3.50E-04	2	0.0012	1					
	Validation		1.64E-04	2	0.001	1					
	Test		3.53E-04	2	0.0011	1					
MRE	Train	Low	2.8854	2	6.4435	1					
	Validation		2.4723	2	5.5861	1					
	Test		3.0775	2	5.8721	1					
Summated score				48		24					

To further assess the statistical significance of performance differences among the predictive models, the Wilcoxon signed-rank test was conducted, and the corresponding p-values are illustrated in Figure 5. The results clearly indicate that the differences between $VAO-DT$ and the benchmark models (SVR, ANN, and RBF) are highly significant, with p-values close to zero (e.g., 1.35E–01 for SVR, 7.05E–23 for ANN, and 1.14E–01 for RBF). Similarly, the $MRFO-DT$ model also demonstrates statistically significant superiority compared to conventional models, as reflected by p-values such as 8.43E–03 (SVR), 2.04E–27 (ANN), and 2.29E–01 (RBF). Notably, the pairwise comparison between $VAO-DT$ and $MRFO-DT$ yielded a p-value of 0.3801, suggesting no statistically significant difference in their performance, which highlights their comparable predictive capability. Overall, these findings validate that both VAO–DT and $MRFO-DT$ significantly outperform traditional approaches (SVR, ANN, and RBF), ensuring robust and reliable prediction outcomes.

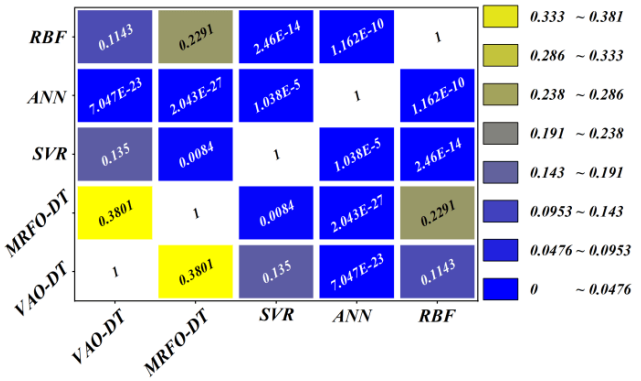

Fig. 5 Pairwise comparison of predictive models using the Wilcoxon signed-rank test

6. Conclusion

The work discussed here focused on identifying and assessing some of the most promising tree-based and machine learning techniques in order to estimate punching shear resistance (V_n) regarding slab-column connections with shear reinforcement. Computer software known as decision tree (DT) analysis is employed in a tree-based manner for this purpose. In this work, DT is hybridized by two metaheuristic optimization techniques to obtain proper values for determining parameters. The first is named Victoria Amazonica Optimization (VAO) and the second is Manta Ray Foraging Optimization ($MRFO$).

The findings suggest that $VAO-DT$ and $MRFO-DT$ can properly predict V_n. The $MRFO-DT$ approach showed good procedure reliability with R^2 values of 0.9826, 0.9893, and 0.9858 in the training, validating, and evaluation phases, respectively. Based on the pattern, $VAO-DT$ surpassed $MRFO-DT$ in R^2 values, with values of 0.9943, 0.9988, and 0.9954.

A study on these parameter values revealed that $VAO-DT$ could produce the minimum values with maximum dependability. The $VAO-DT$ had the lowest RAE index values 0.0274, 0.0191, and 0.0296 during training, validation, and evaluation. The figures were higher accurate throughout learning, validating, and evaluation than $MRFO-DT$'s 0.0589, 0.0554, and 0.0553. For $VAO-DT$, the lowest training, validating, and evaluation $MASE$ index values are 0.04, 0.0292, and 0.0545, respectively. These outcomes were more precise than $MRFO-DT$'s learning, validating, and assessment values of 0.0861, 0.0845, and 0.1019. The $VAO-DT$ has more potential than the $MRFO-DT$ according to level ratings.

The $VAO-DT$ model yields more reliable and robust findings than XGB and $WOA-XGB$, as shown by greater R^2 and lower $RMSE$ and MAE values [Literature]. For $WOA-XGB$, R^2 rose from 0.9642 to 0.9954 during evaluation and from 0.994 to 0.9943 during learning. In addition, $RMSE$ error-based indices reduced from 0.125 to 0.0428 during assessment and from 0.045 to 0.0416 during learning.

All in all, regarding the justifications and explanations, it could be mentioned that although $MRFO-DT$ could receive an acceptable performance, the DT model linked with VAO can be recognized as the most powerful model for prediction purposes, which can be utilized in practical applications.

7. References

A. PD, Jose M, Tiziana R, et al (2018) Experimental Comparison of Novel CFRP Retrofit Schemes for Realistic Full-Scale RC Beam–Column Joints. Journal of Composites for Construction 22:4018027. https://doi.org/10.1061/(ASCE)CC.1943-5614.0000865

Afkhami Hoor S, Esmaeili-Falak M (2024) Innovative Approaches for Mitigating Soil Liquefaction: A State-of-the-Art Review of Techniques and Bibliometric Analysis. Indian Geotechnical Journal. https://doi.org/10.1007/s40098-024-01120-3

Ali AH, Mohamed HM, Chalioris CE, Deifalla A (2021) Evaluating the shear design equations of FRP-reinforced concrete beams without shear reinforcement. Eng Struct 235:112017. https://doi.org/https://doi.org/10.1016/j.engstruct.2021.112017

Alikhani S, Ghiyasi T (2025) Global Energy Transition Influence in Urban Development: Digital Heritage Preservation Methods Approaches. In: After Oil: A Comparative Analysis of Oil Heritage, Urban Transformations, and Resilience Paradigms. Springer, pp 435–454

Bagherabad MB, Rivandi E, Mehr MJ (2025) Machine Learning for Analyzing Effects of Various Factors on Business Economic. Authorea Preprints

Bartolac M, Damjanović D, Duvnjak I (2015) Punching strength of flat slabs with and without shear reinforcement. Građevinar 67:771–786

Ben Chaabene W, Flah M, Nehdi ML (2020) Machine learning prediction of mechanical properties of concrete: Critical review. Constr

Build Mater 260:119889. https://doi.org/https://doi.org/10.1016/j.conbuildmat.2020.119889

Cantone R, Fernández Ruiz M, Bujnak J, Muttoni A (2019) Enhancing punching strength and deformation capacity of flat slabs. ACI Struct J 116:261–274

Dam TX, Wight JK, Parra-Montesinos GJ (2017) Behavior of Monotonically Loaded Slab-Column Connections Reinforced with Shear Studs. ACI Struct J 114:

Dawei Y, Bing Z, Bingbing G, et al (2023) Predicting the CPT-based pile set-up parameters using HHO-RF and PSO-RF hybrid models. Structural Engineering and Mechanics 86:673–686

Deifalla A (2022) Punching shear strength and deformation for FRP-reinforced concrete slabs without shear reinforcements. Case Studies in Construction Materials 16: e00925. https://doi.org/https://doi.org/10.1016/j.cscm.2022.e00925

Deifalla A (2021a) A mechanical model for concrete slabs subjected to combined punching shear and in-plane tensile forces. Eng Struct 231:111787. https://doi.org/https://doi.org/10.1016/j.engstruct.2020.111787

Deifalla A (2021b) A comparative study and a simplified formula for punching shear design of concrete slabs with or without membrane tensile forces. Structures 33:1936–1953. https://doi.org/https://doi.org/10.1016/j.istruc.2021.05.070

Eom T-S, Kang S-M, Choi T-W, Park H-G (2018) Punching shear tests of slabs with high-strength continuous hoop reinforcement. ACI Struct J 115:1295

Erdal HI (2013) Two-level and hybrid ensembles of decision trees for high performance concrete compressive strength prediction. Eng Appl Artif Intell 26:1689–1697. https://doi.org/https://doi.org/10.1016/j.engappai.2013.03.014

Esmaeili-Falak M, Benemaran RS (2024) Ensemble Extreme Gradient Boosting based models to predict the bearing capacity of micropile groups. Applied Ocean Research 151:104149. https://doi.org/https://doi.org/10.1016/j.apor.2024.104149

Esmaeili-Falak M, Katebi H, Vadiati M, Adamowski J (2019) Predicting triaxial compressive strength and Young's modulus of frozen sand using artificial intelligence methods. Journal of Cold Regions Engineering 33:4019007. https://doi.org/https://doi.org/10.1061/(ASCE)CR.1943-5495.0000188

Faridmehr I, Nehdi ML, Hajmohammadian Baghban M (2022) Novel informational bat-ANN model for predicting punching shear of RC flat slabs without shear reinforcement. Eng Struct 256:114030. https://doi.org/https://doi.org/10.1016/j.engstruct.2022.114030

Fazeli Y, Nourbakhsh Z, Yalameha S, Vashaee D (2025) Anisotropic Elasticity, Spin–Orbit Coupling, and Topological Properties of ZrTe2 and NiTe2: A Comparative Study for Spintronic and Nanoscale Applications. Nanomaterials 15:148

Ferreira MP, Melo GS, Regan PE, Vollum RL (2014) Punching of reinforced concrete flat slabs with double-headed shear reinforcement. ACI Struct J 111:363

Gim J, Rhee B (2021) Novel Analysis Methodology of Cavity Pressure Profiles in Injection-Molding Processes Using Interpretation of Machine Learning Model. Polymers (Basel) 13

Goetzke-Pala A, Hoła A, Sadowski Ł (2018) A non-destructive method of the evaluation of the moisture in saline brick walls using artificial neural networks. Archives of Civil and Mechanical Engineering 18:1729–1742. https://doi.org/10.1016/j.acme.2018.07.004

Hassankhani E, Esmaeili-Falak M (2024) Soil-structure interaction for buried conduits influenced by the coupled effect of the protective layer and trench installation. J Pipeline Syst Eng Pract. https://doi.org/https://doi.org/10.1061/JPSEA2/PSENG-1547

Hosseinnia A, Sichani MN, Alamdari BE, et al (2025) Machine Learning Formulation for predicting concrete carbonation depth: A sustainability analysis and optimal mixture design. In: Structures. Elsevier, p 109036

Hugo Dalosto de Oliveira V, Jorge Nery de Lima H, Sales Melo G (2022) Punching shear resistance of flat slabs with different types of stirrup anchorages such as shear reinforcement. Eng Struct 253:113671. https://doi.org/https://doi.org/10.1016/j.engstruct.2021.113671

Jang J-I, Kang S-M (2019) Punching Shear Behavior of Shear Reinforced Slab–Column Connection with Varying Flexural Reinforcement. Int J Concr Struct Mater 13:29. https://doi.org/10.1186/s40069-019-0341-4

Jin Y, Yi WJ, Hu L (2017) Experimental study of performance of reinforced concrete slab-column connection with punching shear keys. Ind Constr 47:60–65

Jumaa GB, Yousif AR (2018) Predicting Shear Capacity of FRP-Reinforced Concrete Beams without Stirrups by Artificial Neural Networks, Gene Expression Programming, and Regression Analysis. Advances in Civil Engineering 2018:5157824. https://doi.org/https://doi.org/10.1155/2018/5157824

Karbassi A, Mohebi B, Rezaee S, Lestuzzi P (2014) Damage prediction for regular reinforced concrete buildings using the decision tree algorithm. Comput Struct 130:46–56. https://doi.org/https://doi.org/10.1016/j.compstruc.2013.10.006

Karimi M, Damirchi F (2025) Re-Evaluating the Functionalist Approach of Urban Management towards Sustainable Architecture and Urban Layout with Emphasis on the Role of Digital Technologies. Journal of Modern Technology 2:327–345

Katariya NK, Choudhary BS, Esmaeili-Falak M, Raina AK (2025) Optimizing open-pit iron ore mine waste dump stability with an increased height: A geotechnical perspective. Geomechanics & engineering 40:69–78

Kinnunen S (2001) Punching of Structural Concrete Slabs: Technical Report. fib Fédération internationale du béton

Kumarawadu H, Weerasinghe P, Perera JS (2024) Evaluating the Performance of Ensemble Machine Learning Algorithms over Traditional Machine Learning Algorithms for Predicting Fire Resistance in FRP Strengthened Concrete Beams. Electronic Journal of Structural Engineering 24:47–53

Lee FL, Park J, Goyal S, et al (2021) Comparison of Machine Learning Methods towards Developing Interpretable Polyamide Property Prediction. Polymers (Basel) 13

Lewiński PM, Więch PP (2020) Finite element model and test results for punching shear failure of RC slabs. Archives of Civil and Mechanical Engineering 20:36. https://doi.org/10.1007/s43452-020-00037-x

Li D, Zhang X, Kang Q, Tavakkol E (2023) Estimation of unconfined compressive strength of marine clay modified with recycled tiles using hybridized extreme gradient boosting method. Constr Build Mater 393:131992. https://doi.org/https://doi.org/10.1016/j.conbuildmat.2023.131992

Liang R, B. Bayrami (2023) Estimation of frost durability of recycled aggregate concrete by hybridized Random Forests algorithms. Steel and Composite Structures 49:91–107. https://doi.org/https://doi.org/10.12989/scs.2023.49.1.091

Lima H, Palhares R, Sales de Melo G, Oliveira M (2021) Experimental analysis of punching shear in flat slabs with variation in the anchorage of shear reinforcement. Structural Concrete 22:1165–1182. https://doi.org/https://doi.org/10.1002/suco.202000158

Manshour S (2025) Utilizing the Potential of Public Spaces for the Development of Urban Leisure and Tourism Areas (Case Study: Zargandeh Neighborhood Central District). Current Opinion 5:1073–1095

Manshour S, Lehmann S (2025) A Systematic Review of Passive Cooling Strategies Integrating Traditional Wisdom and Modern Innovations for Sustainable Development in Arid Urban Environments. arXiv preprint arXiv:250709365

Mellios N, Uz O, Spyridis P (2023) Data-based modeling of the punching shear capacity of concrete structures. Eng Struct 275:115195. https://doi.org/https://doi.org/10.1016/j.engstruct.2022.115195

Metwally IM (2013) Prediction of punching shear capacities of two-way concrete slabs reinforced with FRP bars. HBRC Journal 9:125–133. https://doi.org/https://doi.org/10.1016/j.hbrcj.2013.05.009

Mousavi SMH (2023) Victoria Amazonica Optimization (VAO): an algorithm inspired by the giant water Lily Plant. arXiv preprint arXiv:230308070

Oghli NK, Esmaeili-Falak M (2025) Predicting Liquefaction Triggering Potential Using Metaheuristic GMDH Approaches. Geotechnical and Geological Engineering 43:308. https://doi.org/10.1007/s10706-025-03275-z

Rafiei MH, Adeli H (2017) A novel machine learning-based algorithm to detect damage in high-rise building structures. The Structural Design of Tall and Special Buildings 26:e1400. https://doi.org/https://doi.org/10.1002/tal.1400

Raman RKS, Guo F, Al-Saadi S, et al (2020) Understanding Fibre-Matrix Degradation of FRP Composites for Advanced Civil Engineering Applications: An Overview. Corrosion and Materials Degradation 1:27–41

Rivandi E (2024) FinTech and the level of its adoption in different countries around the world. Available at SSRN 5049827

Rivandi E, Jamili Oskouie R (2024) A Novel Approach for Developing Intrusion Detection Systems in Mobile Social Networks. Available at SSRN 5174811

Salehi H, Burgueño R (2018) Emerging artificial intelligence methods in structural engineering. Eng Struct 171:170–189. https://doi.org/https://doi.org/10.1016/j.engstruct.2018.05.084

Salem NM (2021) A Survey on Various Image Inpainting Techniques. Future Engineering Journal 2:

Salem NM, Mahdi HMK, Abbas H (2018) Semantic Image Inpainting Using Self-Learning Encoder-Decoder and Adversarial Loss. In: 2018 13th International Conference on Computer Engineering and Systems (ICCES). pp 103–108

Sarkhani Benemaran R (2023) Application of extreme gradient boosting method for evaluating the properties of episodic failure of borehole breakout. Geoenergy Science and Engineering 211837. https://doi.org/https://doi.org/10.1016/j.geoen.2023.211837

Shen Y, Wu L, Liang S (2022) Explainable machine learning-based model for failure mode identification of RC flat slabs without transverse

reinforcement. Eng Fail Anal 141:106647. https://doi.org/https://doi.org/10.1016/j.engfailanal.2022.106647

Tamimi MF, Alshannaq AA, Abu Qamar MI (2023) Sensitivity and reliability assessment of buckling restrained braces using machine learning assisted simulation. J Constr Steel Res 211:108187. https://doi.org/https://doi.org/10.1016/j.jcsr.2023.108187

Tran V-L, Kim S-E (2021) A practical ANN model for predicting the PSS of two-way reinforced concrete slabs. Eng Comput 37:2303–2327. https://doi.org/10.1007/s00366-020-00944-w

Turgut OE (2020) A novel chaotic manta-ray foraging optimization algorithm for thermo-economic design optimization of an air-fin cooler. SN Appl Sci 3:3. https://doi.org/10.1007/s42452-020-04013-1

Vaziri NM, Salehipour S (2025) Performance of Lightweight alkali-activated slag concrete before and after exposure to elevated temperatures: mechanical properties and durability. Journal of Building Engineering 113907

Vu D-T, Hoang N-D (2016) Punching shear capacity estimation of FRP-reinforced concrete slabs using a hybrid machine learning approach. Structure and Infrastructure Engineering 12:1153–1161. https://doi.org/10.1080/15732479.2015.1086386

Wu Y, Zhou Y (2023) Prediction and feature analysis of punching shear strength of two-way reinforced concrete slabs using optimized machine learning algorithm and Shapley additive explanations. Mechanics of Advanced Materials and Structures 30:3086–3096. https://doi.org/10.1080/15376494.2022.2068209

Xian G, Guo R, Li C, Hong B (2021) Effects of rod size and fiber hybrid mode on the interface shear strength of carbon/glass fiber composite rods exposed to freezing-thawing and outdoor environments. Journal of Materials Research and Technology 14:2812–2831. https://doi.org/https://doi.org/10.1016/j.jmrt.2021.08.088

Yan H, Xie N, Shen D (2024a) Hybrid Machine Learning Algorithms for Prediction of Failure Modes and Punching Resistance in Slab-Column Connections with Shear Reinforcement. Buildings 14:1247

Yan H, Xie N, Shen D (2024b) Hybrid Machine Learning Algorithms for Prediction of Failure Modes and Punching Resistance in Slab-Column Connections with Shear Reinforcement. Buildings 14:1247

Yang C, Ma W, Zhong J, Zhang Z (2021) Comparative Study of Machine Learning Approaches for Predicting Creep Behavior of Polyurethane Elastomer. Polymers (Basel) 13

Ye Y-Y, Zeng J-J, Li P-L (2022) A State-of-the-Art Review of FRP-Confined Steel-Reinforced Concrete (FCSRC) Structural Members. Polymers (Basel) 14

Zhang K, Zhang Y, Razzaghzadeh B (2024) Application of the optimal fuzzy-based system on bearing capacity of concrete pile. Steel and Composite Structures 51:25–41

Zhao W, Zhang Z, Wang L (2020) Manta ray foraging optimization: An effective bio-inspired optimizer for engineering applications. Eng Appl Artif Intell 87:103300. https://doi.org/https://doi.org/10.1016/j.engappai.2019.103300

Zhu, Y.; Huang, L.; Zhang, Z.; Bayrami B (2022) Estimation of splitting tensile strength of modified recycled aggregate concrete using hybrid algorithms. Steel and Composite Structures 44:389–406. https://doi.org/https://doi.org/10.12989/scs.2022.44.3.389

Disclaimer